Generalized Replica Exchange Method

Jaegil Kim,[a] Thomas Keyes, and John E. Straub

Department of Chemistry, Boston University, Boston, Massachusetts 02215, USA

We present a powerful replica exchange method, particularly suited to first-order phase transitions associated with the backbending in the statistical temperature, by merging an optimally designed generalized ensemble sampling with replica exchanges. The key ingredients of our method are parametrized effective sampling weights, smoothly joining ordered and disordered phases with a succession of unimodal energy distributions by transforming unstable or metastable energy states of canonical ensembles into stable ones. The inverse mapping between the sampling weight and the effective temperature provides a systematic way to design the effective sampling weights and determine a dynamic range of relevant parameters. Illustrative simulations on Potts spins with varying system size and simulation conditions demonstrate a comprehensive sampling for phase-coexistent states with a dramatic acceleration of tunneling transitions. A significant improvement over the power-law slowing down of mean tunneling times with increasing system size is obtained, and the underlying mechanism for accelerated tunneling is discussed. © *2010 American Institute of Physics*. [doi:10.1063/1.3432176]

I. INTRODUCTION

Recently, the temperature replica exchange method[1,2] (*t*REM) [also called parallel tempering[3] (PT)] has become a key workhorse for equilibrium sampling of a variety of complex systems across multidisciplinary fields.[4–8] Simulating a set of replicas of the same system at a distribution of temperatures and swapping configurations among replicas offers an effective means of avoiding trapping in local minima and mitigating broken ergodicity at low temperatures.[9]

A great deal of effort[10–27] has been devoted to improving the efficiency of the standard *t*REM. One of the debated issues is its applicability to systems displaying strong phase transitions, around which metastable or unstable energy states intervene between two macroscopic phases.[28] The standard *t*REM struggles to attain its maximum power in the vicinity of a first-order phase transition, in which canonical energy distributions are effectively disjointed by an energy gap corresponding to a latent heat. Since the acceptance probability of replica exchanges is determined by the energy overlap of neighboring replicas an energy gap between $P_{T<T_c}(E)$ and $P_{T>T_c}(E)$ around the critical temperature T_c, $P_T(E)$ being the canonical probability density function (PDF) at the temperature T, significantly impairs replica exchanges.

More fundamentally, the failure of the *t*REM in first-order phase transitions is intimately connected to an anomalous behavior of the microcanonical entropy, $S(E)$, across the transition region. In many finite size systems, such as spins,[29] nuclei fragmentations,[30,31] model proteins,[32–34] and atomic clusters,[8,35,36] $S(E)$ shows a convex dip, i.e., $\partial^2 S/\partial E^2 > 0$,[30] across the transition region, as sketched in Fig. 1(a). Stemming from this convex "intruder" in $S(E)$, the statistical temperature or microcanonical temperature,

$$T_S(E) = (\partial S/\partial E)^{-1}, \qquad (1)$$

exhibits a negative slope region in Fig. 1(b), the so called backbending or *S*-loop.[32,33,35,36] The existence of the backbending has been verified in recent experiments on nuclear fragmentation[37] and cluster melting,[38] and its physical origin has been attributed to avoiding a "static" phase coexistence due to the free energy cost forming interfaces.

The backbending in $T_S(E)$ manifests a bimodal structure in $P_T(E) \propto e^{-\beta \mathcal{F}(E,T)}$, $\mathcal{F}(E,T)=E-TS(E)$ being the Helmhotz free energy density and $\beta=[k_B T]^{-1}$ $(k_B=1)$.[39] With the stationary points, E_i^*, of $\mathcal{F}(E,T)$ determined by an extremum condition, $T_S(E_i^*)=T$, with $E_1^*<E_2^*<E_3^*$ for $T_2<T<T_1$,[30,34] $P_T(E)$ becomes double peaked at E_1^* and E_3^* with a minimum at E_2^*. The stability condition, $\beta \mathcal{F}''(E)=\beta^2 T_S'(E)$, the prime being a differentiation with respect to E, reveals that the intermediate energy states between E_u^1 and E_u^2 in Fig. 1(b) corresponding to the backbending region in $T_S(E)$ are intrinsically unstable for the canonical ensemble.

For a small system size, L, the canonical ensemble can sample both free energy minima, at E_1^* and E_3^*, across the free energy barrier at E_2^*. However, as L increases, the backbending energy region becomes inaccessible due to a high free energy barrier, implying that tunneling transitions between the two macroscopic phases become unlikely, and $P_T(E)$ becomes localized around E_1^* or E_3^*, depending on whether $T<T_c$ or not. Accordingly, the acceptance of replica exchanges for a pair of inverse temperatures, β and β', close to $\beta_c=1/T_c$, becomes exponentially suppressed as

$$A(\beta E; \beta' E') = \min[1, e^{\Delta \beta(E'-E)}] \approx e^{-|\Delta \beta \Delta E^*|}, \qquad (2)$$

where $\Delta \beta=\beta'-\beta$ and $\Delta E^*=E_3^*-E_1^*$. Notice that $\Delta E=E'-E \approx \Delta E^*$ for $\beta>\beta_c>\beta'$ and $\Delta E \approx -\Delta E^*$ for $\beta<\beta_c<\beta'$ since $P_T(E)$ is centered at E_1^* for $\beta>\beta_c$ and E_3^* for $\beta<\beta_c$. We conclude that the instability of the canonical ensemble to the negative slope region in $T_S(E)$ is the main cause of the poor
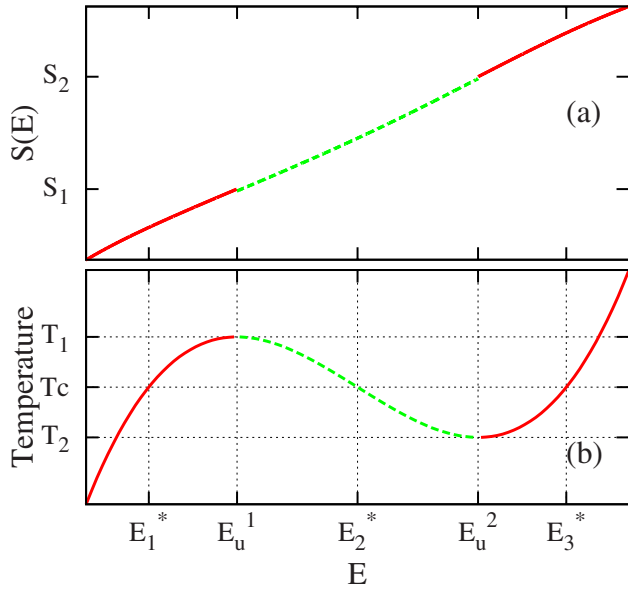
a)Electronic mail: jaegil@bu.edu.

FIG. 1. A schematic representation of (a) the convex dip i.e., $\partial^2 S/\partial E^2 > 0$ in $S(E)$ and (b) the backbending in $T_S(E)$. Intermediate energy states between E_u^1 and E_u^2 are unstable in the canonical ensemble and become inaccessible as the system size increases.

acceptance of replica exchanges in the standard tREM, with increasing system size.

An obvious way to restore the full power of replica exchanges is to utilize a noncanonical ensemble, avoiding the instability to the negative slope region in $T_S(E)$, and allowing a unimodal energy distribution. The Gaussian ensemble approach[40] and its parallel version[41] accomplish this goal by multiplying the Boltzmann factor by a Gaussian in energy.

In this paper, we propose a general framework to systematically build up optimized noncanonical ensembles, transforming unstable or metastable energy states of canonical ensembles into stable states in the presence of the backbending in $T_S(E)$. Exploiting the one-to-one correspondence between the sampling weight and the effective temperatures,[42–46] we develop an inverse mapping strategy, which determines a set of optimal generalized ensemble weights from the parametrized effective temperatures tailored to naturally bridge between ordered and disordered phases via a succession of unimodal energy distributions.

Simulations on Potts spins with varying system size, L, demonstrate that optimally designed generalized ensembles combined with replica exchanges (gREM) yield a dramatic acceleration of tunneling transitions and enable a comprehensive sampling of the phase transition region. A detailed mechanism for an order of magnitude acceleration in tunneling is discussed, with a quantitative performance comparison to the Wang–Landau (WL) method. Finite size scaling analysis reveals that the mean tunneling time, τ_E, can be as favorable as $\propto L^{2d}$ characteristic of a perfect random walk in flat histogram methods.[47–49]

The paper is organized as follows: In Sec. II, the theory of the gREM is presented, with detailed simulation protocols. In Sec. III, the performance of the gREM is examined and quantitatively compared to that of WL sampling,[48] for

Potts spin systems under various simulation conditions. Conclusions and a brief summary are presented in Sec. IV.

II. GENERALIZED REPLICA EXCHANGE METHOD

A. Inverse mapping strategy

The key idea of the gREM is to construct a set of generalized ensemble weights, $W_\alpha(E,\lambda_\alpha)$ ($\alpha = 1, 2, \ldots, M$), which, as the parameter λ_α varies, successively access the unstable energy region between E_u^1 and E_u^2 in Fig. 1(b). Here α and M are the replica index and the number of replicas, respectively. An important relation in the design of optimal weights is the inverse mapping between the W_α and the effective temperature

$$T_\alpha(E;\lambda_\alpha) = [\partial w_\alpha/\partial E]^{-1}, \tag{3}$$

$w_\alpha = -\ln W_\alpha$ being the generalized effective potential. Notice that the definition of the effective temperature in Eq. (3) is analogous to that of the statistical temperature in Eq. (1). Based on the one-to-one correspondence in Eq. (3), the effective temperature completely determines the sampling weight up to a constant through the inverse mapping,

$$w_\alpha(E;\lambda_\alpha) = \int^E 1/T_\alpha(z;\lambda_\alpha)dz. \tag{4}$$

A necessary and sufficient condition on $T_\alpha(E;\lambda_\alpha)$, such that unstable or metastable energy states of the canonical ensemble between E_u^1 and E_u^2 are transformed into stable ones with a unimodal PDF, is derived by identifying an extremum, E_α^*, of a generalized free energy density, $\beta\mathcal{F}_\alpha(E) = w_\alpha(E) - S(E)$,

$$T_\alpha(E_\alpha^*;\xi_\alpha) = T_S(E_\alpha^*) = T_\alpha^*, \tag{5}$$

and a stability condition

$$\beta\mathcal{F}_\alpha''(E_\alpha^*) = (\gamma_S - \gamma_\alpha)/T_\alpha^{*2}, \tag{6}$$

where $\gamma_S = T_S'(E_\alpha^*)$ and $\gamma_\alpha = T_\alpha'(E_\alpha^*)$, and the prime denotes differentiation with respect to E. The primary finding in both Eqs. (5) and (6) is that the stationary points of $\mathcal{F}_\alpha(E)$, E_α^*, are determined as the crossing points between $T_\alpha(E;\lambda_\alpha)$ and $T_S(E)$ in two-dimensional (E,T) space, and the parameter γ_α modulates the stability of E_α^* via $\gamma_\alpha = T_\alpha'(E_\alpha^*;\lambda_\alpha)$. Based on Eqs. (5) and (6) we find that a unimodal distribution in the generalized PDF (GPDF), i.e., $P_\alpha(E) = e^{-\beta\mathcal{F}_\alpha}$, can arise from forming the unique crossing point, E_α^*, between $T_S(E)$ and $T_\alpha(E;\lambda_\alpha)$, subject to $\gamma_\alpha(E_\alpha^*) < \gamma_S(E_\alpha^*)$.

More quantitatively, expanding the GPDF up to second order yields

$$P_\alpha(E;\lambda_\alpha) \approx \exp\{-(E - E_\alpha^*)^2/2\sigma_\gamma\}, \tag{7}$$

$\sigma_\gamma = T_\alpha^{*2}/(\gamma_S - \gamma_\alpha)$, illuminating that the "stable" in Fig. 2, with $\gamma_\alpha < \gamma_S$, generates a Gaussian PDF centered at E_α^* with the positive σ_γ even for a negative γ_S. As γ_α further decreases to $-\infty$, the Gaussian in Eq. (7) approaches $\delta(E - E_\alpha^*)$ corresponding to the microcanonical ensemble case. On the other hand, $P_\alpha(E)$ becomes locally flat around E_α^*, with $\gamma_\alpha = \gamma_S$ ("marginal" in Fig. 2). The crossing point, E_α^*, becomes unstable for $\gamma_\alpha > \gamma_S$ as in the canonical ensemble.
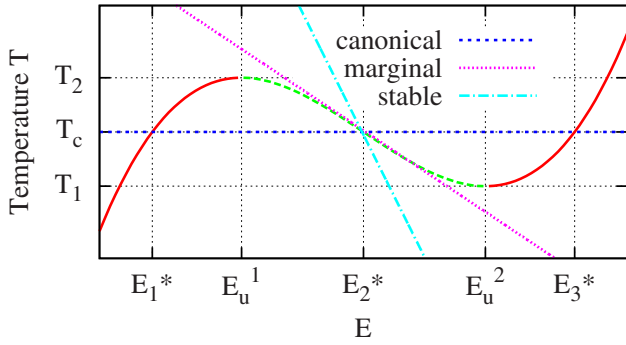
FIG. 2. Statistical temperature $T_S(E)$ and effective temperatures $T_\alpha(E) = T_c + \gamma_\alpha(E - E_2^*)$ with varying γ_0, $\gamma_0 = T_\alpha'(E_2^*)$. Unstable energy states around E_2^* in the canonical ensemble ($\gamma_0 = 0$) become stable in the generalized ensemble of Eq. (10) with $\gamma_0 < \gamma_S^{min} = T_S'(E_2^*)$. Marginal corresponds to $\gamma_0 = \gamma_S^{min}$.

B. Linear effective temperature: Tsallis weight

The simplest parametrization scheme for forming stable crossing points between $T_\alpha(E; \lambda_\alpha)$ and $T_S(E)$ is to align linear effective temperatures in parallel with the constant slope, λ_0 [see Fig. 3(a)], as

$$T_\alpha(E; \lambda_\alpha) = \lambda_\alpha + \gamma_0(E - E_0), \tag{8}$$

the control parameter λ_α being the T-intercept at an arbitrarily chosen E_0. To form the unique stable crossing point E_α^* in each replica, γ_0 must be less than the minimum slope γ_S^{min}, $\gamma_S^{min} = \min\{T_S'(E)\}$ being the minimum slope of $T_S(E)$ for the sampled energy region. Since $T_S(E)$ is monotonically increasing except for the transition region, in most cases a proper γ_0 is easily guessed from the approximate $T_S(E)$ by connecting a few points of $[\tilde{U}(T), T]$, $\tilde{U}(T)$ being an average energy of a short canonical run at T. For example, γ_0 can be simply chosen as $\gamma_L = (T_M - T_1)/(\tilde{U}_1 - \tilde{U}_M)$, T_1 and T_M being the lowest and highest temperature, and $\tilde{U}_\alpha = \tilde{U}(T_\alpha)$.

Once γ_0 is fixed the dynamic range of λ_α is determined to cover the interesting temperature range between T_1 and T_M as $\lambda_1 = T_1$ and $\lambda_M = T_M - \lambda_0(\tilde{U}_M - \tilde{U}_1)$, with $E_0 = \tilde{U}_1$. The first and Mth effective temperatures are chosen to cross $[\tilde{U}_1, T_1]$ and $[\tilde{U}_M, T_M]$, respectively. Then, the intermediate values of λ_α ($1 < \alpha < M$) are determined by equally dividing the parameter space as

$$\lambda_\alpha = \lambda_1 + (\alpha - 1)\Delta\lambda \tag{9}$$

and $\Delta\lambda = (\lambda_M - \lambda_1)/(M - 1)$.

Interestingly, the linear effective temperature of Eq. (8) produces a generic form of the Tsallis weight[50–52]

$$W_\alpha(E; \lambda_\alpha) \sim [\lambda_\alpha + \gamma_0(E - E_0)]^{-1/\gamma_0}. \tag{10}$$

Identifying γ_0 and λ_α by $(q - 1)$ and β_α^{-1}, respectively, q being the nonextensivity parameter, recovers the original form of the Tsallis weight proposed in nonextensive statistical mechanics.[50] Thus the gREM with the linear effective temperature of Eq. (8) is basically equivalent to the Tsallis-weight based REM, previously presented in the form of the generalized PT,[14] q-REM,[15] and Tsallis-REM.[53]

However, it should be noted that the parametrized Tsallis weights in the gREM are targeted to transform unstable and
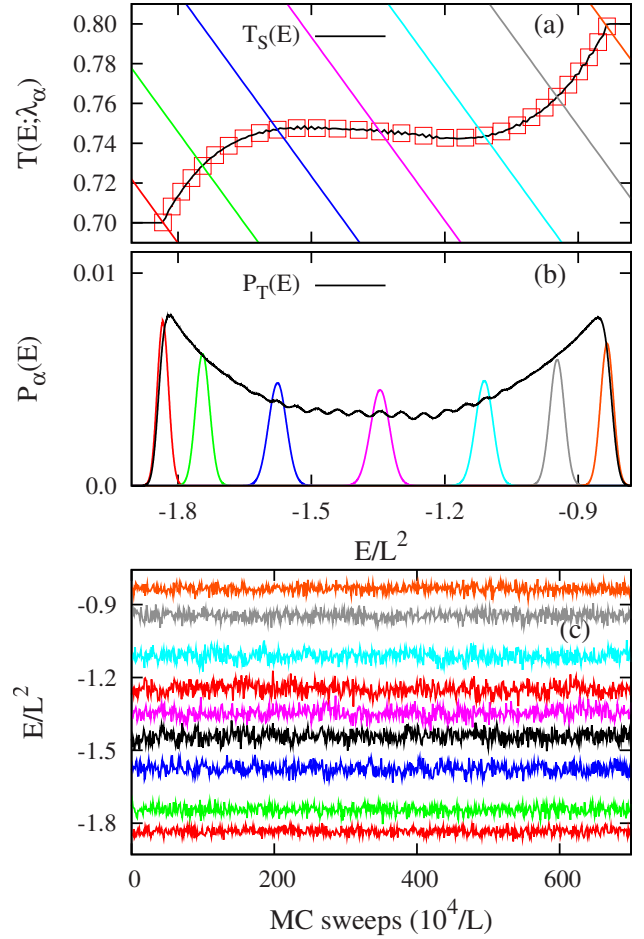

FIG. 3. (a) Most probable energy set $[E_\alpha^*, T_\alpha^*]$ (squares) determined by the gREM$_3$ for 10^7 MCS and $T_S(E)$ (solid line) determined by the STMC simulation and effective temperatures $T_\alpha(E; \lambda_\alpha)$, (b) resulting GPDFs $P_\alpha(E)$ and $P_T(E)$ (solid line) for Potts spins with $L = 64$, and (c) energy trajectories sampled by Eq. (10). In both (a) and (b), $\alpha = 1, 5, 10, 15, 20, 25,$ and 30 from left to right. $\alpha = 1, 5, 10, 13, 15, 17, 20, 25,$ and 30 from down to up in (c).

metastable energy states of the canonical ensemble into stable ones, resulting in much narrower energy distributions than the canonical PDFs. On the other hand, other variants[14,15,53,54] of the Tsallis-weight based REM are mainly focused on producing more delocalized energy distributions to increase an acceptance of replica exchanges. This is why the gREM utilizes λ_α as a control parameter rather than q in the conventional implementation.

Another advantage of the gREM is that the inverse mapping enables a systematic selection of relevant parameters, which is particularly beneficial for the negative slope region of $T_S(E)$. The dynamic range of λ_α lies between λ_1 and λ_M determined by two short canonical runs at T_1 and T_M, respectively. The inverse mapping is a general framework for the combination of any generalized ensemble sampling with replica exchanges. Depending on the profile of $T_S(E)$, characteristic of the phase transition, different types of effective temperatures can be designed to produce optimal weights. In the limit, $\gamma_0 \to 0$, the gREM recovers the tREM running on temperatures λ_α, denoting $W_\alpha(E; \lambda_\alpha) \sim e^{-(E - E_0)/\lambda_\alpha}$.

C. Simulation protocols of the gREM

Detailed simulation protocols of the gREM are outlined as follows.

TABLE I. Simulation parameters and mean tunneling times τ_E for the gREM and the WL simulations for Potts spins with $L=64$. t_S represents a total simulation time in the gREM and a time spent for refining $\widetilde{S}(E)$ up to $f_d=10^{-9}$ in the WL. The gREM$_i^*$ simulations are associated with Eq. (13) based on $[E_\alpha^*,T_\alpha^*]$ determined by the gREM$_3$.

Methods	L	M	γ_0	E_0	τ_E (MCS)	t_S (MCS) ($\times 10^8$)
gREM$_1$	64	30	-0.000010	-1.83	193.0	1.5
gREM$_2$	64	30	-0.000025	-1.83	388.5	1.5
gREM$_3$	64	30	-0.000075	-1.83	1511.5	1.5
gREM$_4$	64	30	-0.00015	-1.83	3950.8	1.5
gREM$_1^*$	64	30	-0.0000075	-1.83	390.6	1.5
gREM$_2^*$	64	30	-0.000015	-1.83	739.4	1.5
gREM$_3^*$	64	30	-0.000075	-1.83	1553.7	1.5
WL	64				2.34×10^5	1.53

(i) Perform short canonical runs at several temperatures between T_1 and T_M to determine the data set, $[\widetilde{U}_\alpha, T_\alpha]$. Select a proper γ_0 to be less than $\gamma_S^{\min}$ and determine λ_α by employing Eq. (9) between $\lambda_1=T_1$ and $\lambda_M=T_M-\gamma_0(\widetilde{U}_M-\widetilde{U}_1)$, with $E_0=\widetilde{U}_1$.

(ii) Run the gREM simulation in each replica by making trial moves in configuration space with the acceptance,

$$A_{\text{intra}}(\mathbf{x} \to \mathbf{x}') = \min[1, e^{w_\alpha(E)-w_\alpha(E')}]. \qquad (11)$$

Every fixed time step, attempt a replica exchange between neighboring replicas with the acceptance

$$A_{\text{inter}}(\alpha;\mathbf{xx}') = \min[1, \exp(\Delta_\alpha)],$$

$$\Delta_\alpha = w_{\alpha+1}(E') - w_{\alpha+1}(E) + w_\alpha(E) - w_\alpha(E'). \qquad (12)$$

(iii) Once a sufficiently long production run has been performed, calculate the entropy estimate $\widetilde{S}(E)$ by joining multiple generalized ensemble runs via the weighted histogram analysis method (WHAM).[55]

III. NUMERICAL SIMULATIONS AND RESULTS

To illustrate how effectively the gREM works around a typical first-order transition, we have chosen eight-state Potts spins as a benchmark, with the energy $E=-\Sigma_{\langle ij \rangle}\delta(S_i,S_j)$,[56] in which the sum runs over the nearest-neighbor spins on an $L\times L$ square lattice and Kronecker δ takes the value one if $S_i=S_j$ and zero otherwise. Here $S_i=1,2,\dots,Q=8$ are spin variables.

A. Characteristic features of the gREM

To determine the dynamic range of λ_α and the optimal value of γ_0 we first performed short canonical Monte Carlo (MC) simulations for 2×10^4 MC sweeps (MCSs) at $T_1=0.7$ and $T_M=0.8$, which determine $\widetilde{U}_1=-7507.8$ and $\widetilde{U}_M=-3438.7$. Here one MCS means L^2 MC trial moves of all spins. Based on $\gamma_L=(T_M-T_1)/(\widetilde{U}_1-\widetilde{U}_M)\approx-2.5\times10^{-5}$ we performed various gREM simulations with varying γ_0 for $L=64$, as summarized in Table I. Replica exchanges were attempted every L MC moves and the ground state was used as the initial configuration in all replicas.

Setting $E_0=\widetilde{U}_1$ in Eq. (8), the dynamic range of λ_α, between $\lambda_1=T_1$ and $\lambda_M=T_M-\gamma_0(\widetilde{U}_M-\widetilde{U}_1)$, depends on γ_0. For $\gamma_0=-0.000\,075$ corresponding to the gREM$_3$ in Table I, $\lambda_1 \approx 0.7$ and $\lambda_M \approx 1.1$. Resulting effective temperatures (solid lines) in Fig. 3(a) are chosen to fully cover the phase transition region, including the backbending region between $E_u^1 \approx -1.5L^2$ and $E_u^2 \approx -1.15L^2$ in $T_S(E)$. For comparison, we also plot the exact $T_S(E)$, which was determined by the statistical temperature Monte Carlo (STMC) algorithm[49] for 2×10^8 MCS. All relevant parameters in the gREM$_3$ have been chosen based on short canonical runs at T_1 and T_M and full knowledge of $T_S(E)$ is not necessary.

Since $T_\alpha(E;\lambda_\alpha)$ was designed to form a unique, stable crossing point, E_α^*, with $T_S(E)$, the resulting GPDFs in Fig. 3(b) are rapidly localized around E_α^* with a Gaussian shape, and naturally bridge between ordered and disordered phases with uimodal energy distributions across the transition region. Since $P_\alpha(E)$ is sharply peaked at E_α^*, $T(E_\alpha^*;\lambda_\alpha) = T_S(E_\alpha^*)$, the set of most probable energies, $[E_\alpha^*,T_\alpha^*]$, asymptotically converge toward a locus of $T_S(E)$. Indeed, the profile of $[E_\alpha^*,T_\alpha^*]$ shows a perfect coincidence with $T_S(E)$ determined by STMC, and exactly correspond to crossing points between $T_S(E)$ and $T_\alpha(E;\lambda_\alpha)$ in Fig. 3(a). For convenience, the most probable energy E_α^* was approximated by the average energy summed over the αth replica.

The superimposed energy distribution, $P_T(E) = (1/M)\Sigma_\alpha P_\alpha(E)$, shows an almost uniform sampling across the backbending region with a characteristic structure, resulting from narrowly peaked $P_\alpha(E)$. Each energy trajectory sampled by $W_\alpha(E;\lambda_\alpha)$ in Fig. 3(c) is constantly fluctuating around E_α^*, explicitly illustrating that the gREM achieves a comprehensive sampling for phase-coexistent states by transforming unstable energy states of the canonical ensembles into stable ones.

Actual replica trajectories initiated from $\alpha=1$ and 30 in Figs. 4(a) and 4(b) start to sample the whole dynamic energy range after 3×10^4 MCS and exhibit very frequent tunneling transitions in both energy and replica spaces via the localized GPDFs across the transition region. For comparison we also performed a tREM simulation with $M=30$, employing an equidistant temperature allocation for the same temperature range between T_1 and T_M. Two effectively disjointed sampling domains with no replica exchanges around $\alpha=14$ are
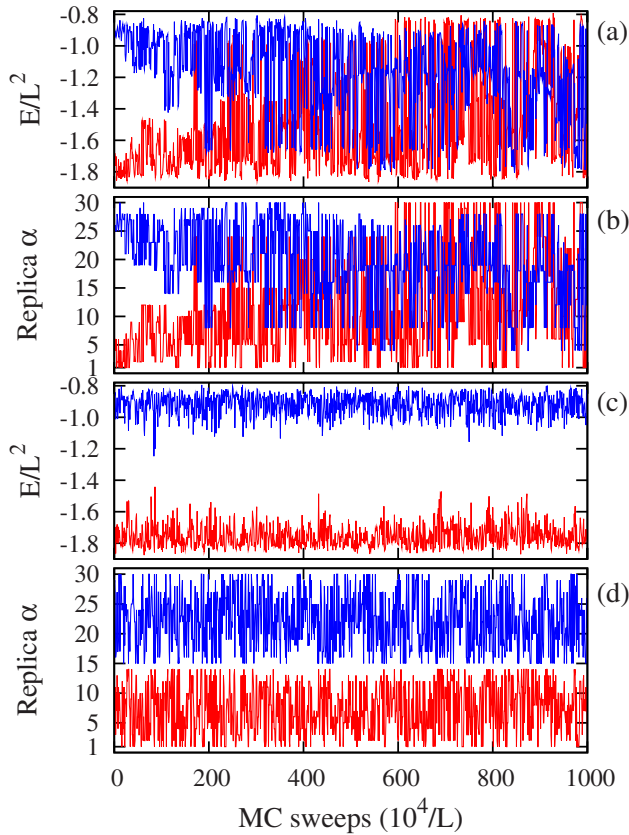
FIG. 4. Simulated trajectories of $\alpha=1$ and 30 in (a) energy and (b) replica space of the gREM$_3$, and in (c) energy and (d) replica space of the tREM for Potts spins with $L=64$.

apparent in Figs. 4(c) and 4(d) due to a vanishing energy overlap between far-separated energy distributions of neighboring replicas at T_c.

B. γ_0 dependence of the gREM

Varying γ_0 directly affects the gREM simulation by changing the width of GPDFs and the distribution of E_α^*. These effects are entangled in Eq. (8) since decreasing γ_0 produces a more dense population of E_α^* for the transition region, as demonstrated in Fig. 5(a), but a narrower GPDF in each replica due to the increased $\sigma_\gamma = T_\alpha^{*\,2}/(\gamma_S - \gamma_0)$. The collapse of $[E_\alpha^*, T_\alpha^*]$ of both gREM$_1$ and gREM$_4$ into $T_S(E)$ determined by STMC reveals that the most probable energy set indeed traces a locus of $T_S(E)$.

Due to the opposing effects of γ_0 for energy overlaps between neighboring replicas, the acceptance probability, $p_{\rm acc}(\alpha)$, for replica exchanges between α and $(\alpha+1)$ shows a nonmonotonic γ_0-dependence in Fig. 5(b). The tREM shows no replica exchanges around $T_c \approx 0.745\,46$, with a minimum in $p_{\rm acc}(\alpha)$ at $\alpha=14$ ($T_{14}=0.7448$ and $T_{15}=0.7482$). On the other hand, a systematic enhancement of $p_{\rm acc}(\alpha)$ shows up around $\alpha=14$ in the gREM as the effective temperatures form stable crossing points in the transition region, upon decreasing γ_0 to $-0.000\,025$. A further decrease to $\gamma_0 = -0.000\,15$ yields an almost uniform acceptance, but an overall reduction in $p_{\rm acc}(\alpha)$ due to significantly narrowed GPDFs.

The γ_0-dependence of the gREM is also clearly captured in the superimposed energy distributions, $P_T(E)$, in Fig. 5(c),
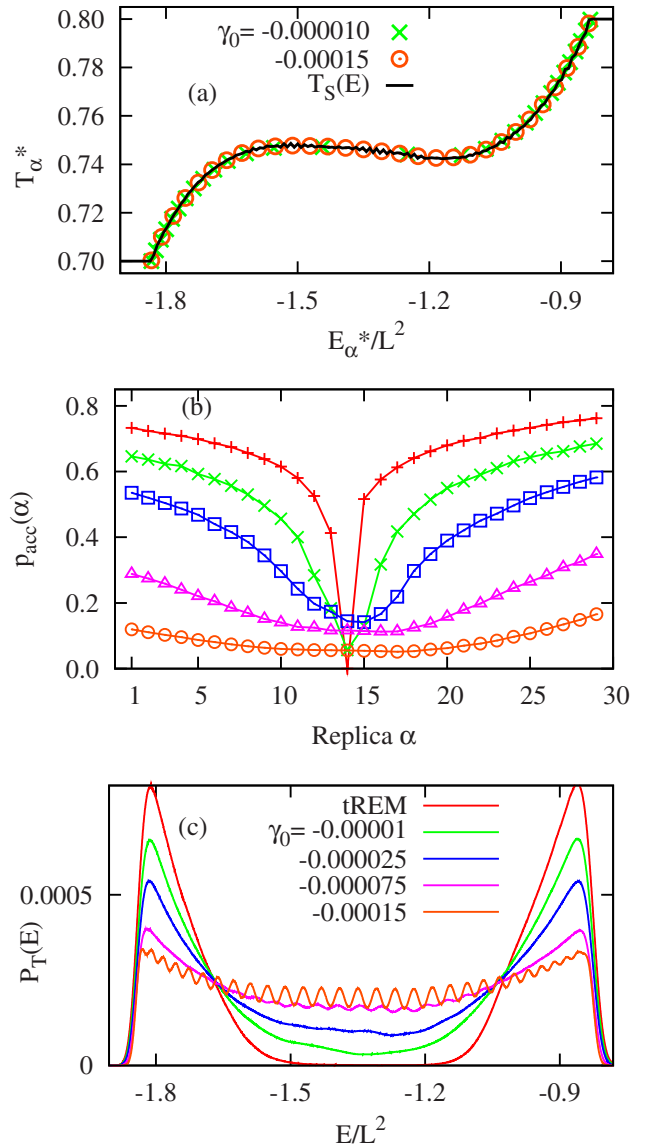

FIG. 5. (a) Most probable energy set $[E_\alpha^*, T_\alpha^*]$ of the gREM$_1$ and the gREM$_4$ simulations, (b) acceptances probabilities $p_{\rm acc}(\alpha)$, and (c) superimposed energy distributions $P_T(E)$ of various gREM simulations in Table I with varying γ_0 for fixed $L=64$. Same colors are used for the same simulations in both (b) and (c).

illustrating that phase-coexistent energy states between $-1.5L^2$ and $-1.1L^2$ are only accessible for $\gamma_0 < \gamma_S^{\min} \approx -0.000\,005$. The existence of the threshold value $\gamma_S^{\min}$ reveals that the success of the gREM relies on the transformation of unstable energy states of canonical ensembles into stable ones with optimized noncanonical ensembles. As steeper effective temperatures produce a denser population of E_α^* in the transition region, $P_T(E)$ becomes more flattened for the entire energy range, with characteristic oscillatory structures, stemming from sharply peaked $P_\alpha(E)$ as in the gREM$_4$.

Forming more stable crossing points, E_α^*, in the transition region is crucial for sampling phase-coexistent states and smoothly joining ordered and disordered phases in the gREM. However, narrowed GPDFs with decreasing γ_0 is not desirable for $p_{\rm acc}(\alpha)$, as shown in Fig. 5(a). To resolve this
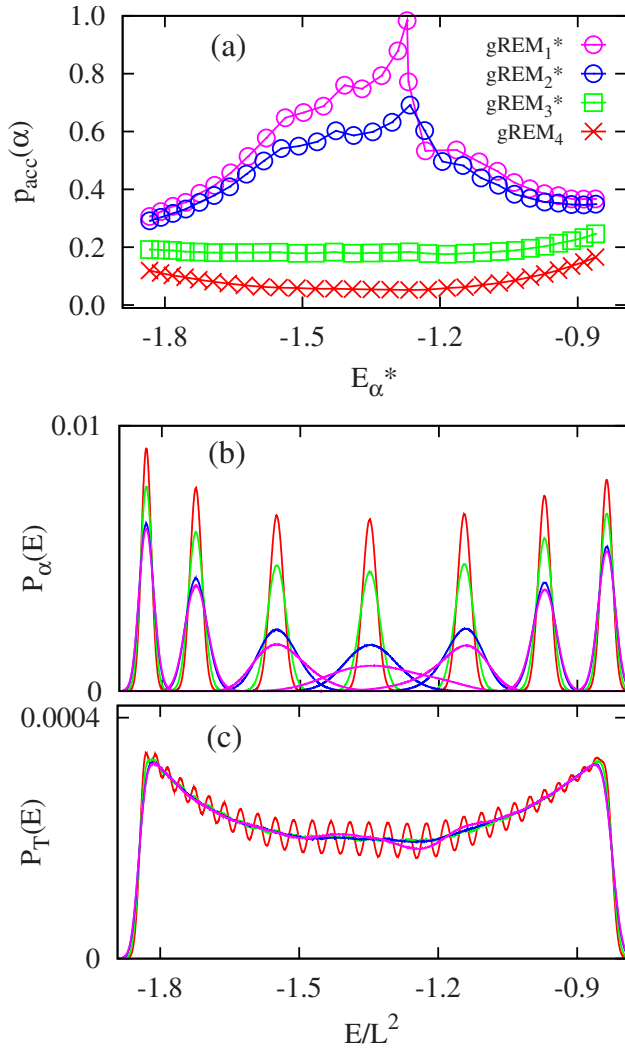
FIG. 6. (a) $p_{acc}(\alpha)$ as a function of E_α^*, (b) resulting GPDFs, and (c) superimposed $P_T(E)$ of the gREM* simulations in Table I for $L=64$. In (b), α =1, 5, 10, 15, 20, 25, and 30 from left to right.

FIG. 7. Accumulated tunneling transitions: N_E as a function of a total MCS in (a) the gREM and (b) the gREM* simulations in Table I for $L=64$. In (a), N_E of the WL has been magnified by 400 times for visualization and the gREM* simulations in (b) were performed with $T_\alpha^*(E;\lambda_\alpha^*)$ based on $[E_\alpha^*, T_\alpha^*]$ of the gREM$_4$.

problem we performed additional simulations, denoted by the gREM* in Table I, employing new effective temperatures as

$$T_\alpha^*(E;\lambda_\alpha^*) = \lambda_\alpha^* + \gamma_0(E - E_0) = T_\alpha^* + \gamma_0(E - E_\alpha^*), \quad (13)$$

with $\lambda_\alpha^* = T_\alpha^* - \gamma_0(E_\alpha^* - E_0)$. In Eq. (13), newly assigned control parameters λ_α^* make $T_\alpha^*(E;\lambda_\alpha^*)$ cross the most probable energy set $[E_\alpha^*, T_\alpha^*]$ of the gREM$_4$, maintaining a dense population of E_α^* for the transition region irrespective of γ_0.

As seen in Fig. 6(a), a significant enhancement of $p_{acc}(\alpha)$, with an overall uniform acceptance, is obtained for gREM$_3^*$, in comparison with gREM$_3$, even with the same $\gamma_0 = -0.000\,075$. The increase in $p_{acc}(\alpha)$ for the transition region is more dramatic with a lower γ_0, as in gREM$_1^*$ and gREM$_2^*$, corresponding to $\gamma_0 = -0.000\,007\,5$ and $-0.000\,015$, respectively. The systematic increase in $p_{acc}(\alpha)$ is mainly due to more delocalized GPDFs in the gREM* simulations with increasing γ_0, while maintaining centers of Gaussians at nearly the same E_α^*, as illustrated in Fig. 6(b). More delocalized energy distributions maximize energy overlaps among replicas, leading to a significant accelerati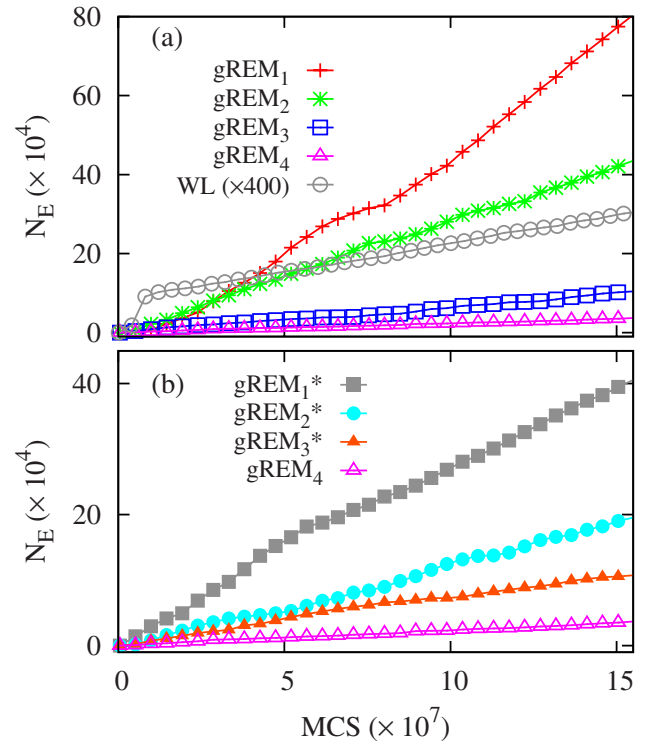on of replica exchanges. As a result, the uniform energy sampling in $P_T(E)$ remains unchanged in Fig. 6(c) regardless of γ_0 and oscillatory structures are smoothed out. This implies that an optimal performance of the gREM is achieved by first determining densely populated $[E_\alpha^*, T_\alpha^*]$ with a steeper γ_0 and then switching to a production run with Eq. (13) at $\gamma_0 \simeq \gamma_S^{min}$.

C. Accelerated tunneling transitions

To systematically quantify the performance of the gREM simulations we compute the number of tunneling transitions in energy, denoted by N_E, measuring how often all replicas make transitions from one phase to the other.[25,47,53,57,58] We also calculate the mean tunneling time, τ_E, by determining the inverse of a linear slope of N_E in production phases of the gREM simulations. Tunneling transitions were counted between the two boundary energies of $-1.80L^2$ and $-0.85L^2$.

Except for an equilibration stage, N_E in Fig. 7(a) is linearly increasing as a function of the total simulation time. This implies that barrier crossing rates, which are proportional to the slope of N_E, are almost constant throughout the simulations. The most frequent tunneling transitions were observed in gREM$_1$ with $\gamma_0 = -0.000\,01$, and N_E systematically decreases as γ_0 decreases from γ_S^{min}, even with a more comprehensive sampling and a better $p_{acc}(\alpha)$ for the phase transition region in Figs. 5(a) and 5(b).

The attenuation of N_E with decreasing γ_0 is mainly due to the increased number of intermediate replicas in the transition region, causing tunneling to require more consecutive replica exchanges. On the other hand, tunneling in the gREM
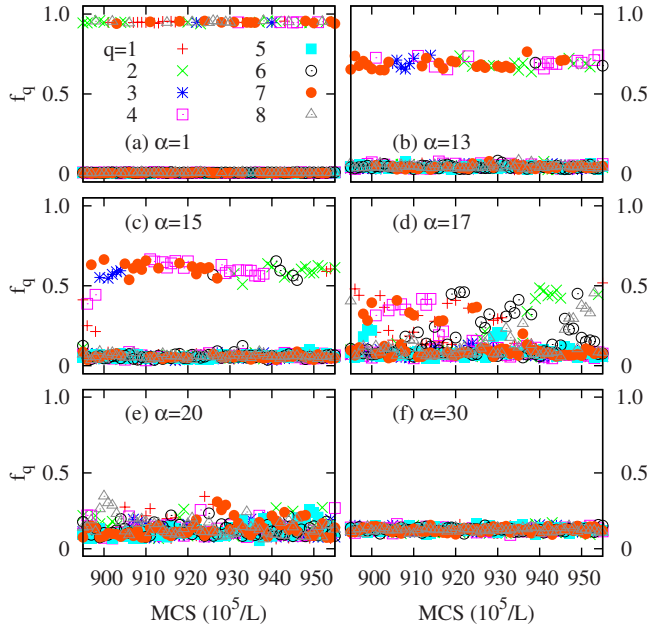
FIG. 8. Time profiles of $f_q = \Sigma_i \delta(S_i, q)/L^2$ in the $g\text{REM}_3$ in Table I for $L = 64$. Notice that intermediate replicas of $\alpha = 13$, 15, and 17 exclusively sample mixed-phase configurations consist of a major spin state with $f_q > 0$ and other minor spin states with $f_q \approx 0$.

with γ_0 close to $\gamma_S^{\min}$ is rather rapid since a couple of replica exchanges among sparsely distributed intermediate replicas leads to a tunneling even with a relatively poor $p_{\text{acc}}(\alpha)$. However, the accelerated N_E with $\gamma_0 \approx \gamma_S^{\min}$ does not necessarily lead to an enhanced convergence because the transition region is poorly sampled due to a lack of replicas, as seen in $P_T(E)$ of Fig. 5(c).

The effect of γ_0 on N_E is more apparent in the $g\text{REM}^*$ simulations in Fig. 7(b), in which the location of intermediate replicas around the transitions region is almost frozen. As expected, increasing γ_0, yielding more delocalized GPDFs centered at the same E_α^* of the $g\text{REM}_4$, results in a monotonic acceleration of N_E, while retaining a faithful sampling in the transition region even with γ_0 close to $\gamma_S^{\min}$. Approximately a tenfold speedup of N_E is observed in $g\text{REM}_1^*$ compared to $g\text{REM}_4$.

For a comparison we also performed the entropic version of the WL sampling[48] for the energy range between $-1.83L^2$ and $-0.83L^2$. The entropy estimate $\widetilde{S}(E)$ has been refined up to $f_d = f - 1 = 10^{-9}$, employing the dynamic update scheme $\widetilde{S}(E) = \widetilde{S}(E) + \ln f$. Following the original convention, the modification factor was reduced to $\sqrt{f}$ once $|H(E) - \bar{H}|/\bar{H} \leq 0.2$, starting from 1.01, with $\bar{H}$ being the average energy histogram. Tunneling transitions in Fig. 7(a), which has been magnified 400 times for visualization, show a steep rise at the initial stage of simulation, in which the nonvanishing

modification factor $\ln f$ constantly biases the system to move away from visited energy regions. The reduction in f is very rapid initially, and f_d reaches 10^{-6} after 3.3×10^7 MCS, but significantly slows down as f_d becomes smaller, resulting in a total of 1.5×10^8 MCS up to $f_d = 10^{-9}$.

The most remarkable point in Fig. 7(a) is the dramatic acceleration of N_E in the $g\text{REM}$ simulations over the WL. Examining the τ_E, in Table I, reveals a speedup of tunneling transitions in the poorest case of our algorithm ($g\text{REM}_4$) of almost 60 times, increasing up to about 150 times for $g\text{REM}_3$. The acceleration of N_E is more significant for the $g\text{REM}^*$ simulations, in which replicas are more densely populated for the backbending region regardless of γ_0 with Eq. (13). The ratio of tunneling times, $R_\tau = \tau_E^{\text{WL}}/\tau_E^{g\text{REM}}$, is about 600 in the $g\text{REM}_1^*$. Here we only considered the simulations having a comprehensive sampling for the transition region, as in WL sampling.

What is the underlying mechanism for an order of magnitude acceleration of N_E in the $g\text{REM}$ over the WL? The bottleneck of barrier crossings in Potts spins is the formation of phase-coexistent states with interfacial regions, which becomes exponentially suppressed in the canonical ensemble. Flat histogram methods such as the multicanonical (MUCA) sampling,[47] WL,[48] and STMC (Ref. 49) alleviate this exponential slowing down by enhancing mixed-phase configurations, employing a sampling weight inversely proportional to the density of states. However, in a single replica simulation of the flat histogram type, forming mixed-phase configurations starting from ordered or disordered phases is intrinsically sequential and cumulative, and τ_E is mainly limited by the diffusion rate in energy space.

On the other hand, some intermediate replicas located at the transition region in the $g\text{REM}$ always retain phase-coexistent states and naturally bridge the ordered and disordered phases through replica exchanges, as illustrated in Figs. 8(a)–8(f), in which fractions of spin states, $f_q = \Sigma_i \delta(S_i, q)/L^2$, in the $g\text{REM}_3$, were plotted as a function of MCS for different α. In the ordered phase ($\alpha = 1$), most spins occupy a single spin state, while all spin states are equally probable in the disordered phase ($\alpha = 30$). Intermediate replicas of $\alpha = 13$, 15, and 17 exclusively sample mixed-phase configurations characterized by a majority state with $f_q > 0.5$ and other states with $f_q \approx 0$; these mixed-phase states are preserved throughout the simulation. We conclude that the main limiting factor for tunneling in the $g\text{REM}$ is the efficacy of replica exchanges among intermediate replicas sampling phase-coexistent states.

D. Scaling behavior of τ_E and $T_S(E)$

In a completely unbiased random walk in energy, corresponding to an ideal limit of flat histogram methods, τ_E

TABLE II. Mean tunneling times τ_E and simulations times t_S of the WL simulations with varying L. Entropy estimates were refined up to $f_d = 10^{-9}$.

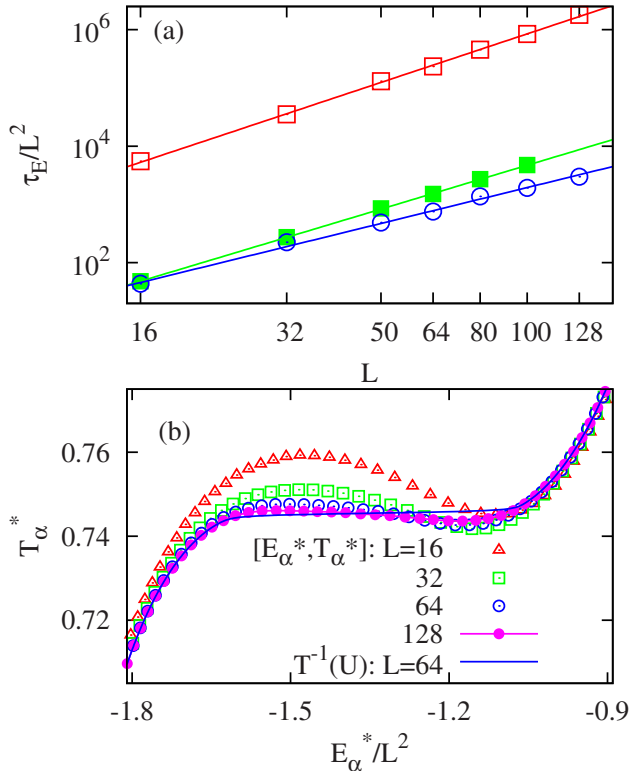| L	16	32	50	64	80	100	128
τ_E ($\times 10^5$) (MCS)	0.055	0.35	1.31	2.34	4.52	8.44	18.12
t_S ($\times 10^7$) (MCS)	0.98	3.16	7.47	1.51	1.69	24.5	32.2

FIG. 9. (a) Log-log plots of mean tunneling times τ_E and L for the WL, and the gREM^I and the gREM^{II} simulations from top to bottom, and (b) profiles of $T_S(E)$ estimated by $[E_\alpha^*, T_\alpha^*]$ of the gREM^{II} simulations with varying L. In (a), lines are linear fits to the corresponding data points.

scales as L^{2d}, with d being the dimension of the system ($d = 2$ in this paper), since the dynamic energy range expands as L^d. In an actual simulation, τ_E scales like L^{2d+z} due to a deviation from a perfect random walk.[47,57] The value of z depends on the system and is known to be 0.65 for Potts spins and 0.73 for Ising spins, from studies using the MUCA (Ref. 47) and the flat histogram sampling exploiting the exact $S(E)$,[57] respectively.

As summarized in Table II, we performed several WL simulations, varying L from 16 to 128. The dynamic energy range was restricted between E_1^* and E_M^* determined by the gREM simulation at the same L. A similar scaling behavior $\tau_E^{WL} \simeq 2.44 \times L^{2d+0.77}$ appears in the WL simulation for Potts spins, as seen in Fig. 9(a), in which the log-log plot of τ_E and L shows a clear linear relationship. A slightly larger exponent

of $z = 0.77$, in comparison with that of the MUCA,[47] might be due to the difference in energy boundaries for tunneling. In our study, transitions were counted between E_1^* and E_M^*, but tunneling transitions in the MUCA were counted between two free energy maxima at T_c, which have a much smaller separation.

To examine scaling properties of the gREM we performed two different sets of simulations with varying L, as summarized in Table III. Simulations in set I denoted by gREM^I are associated with the effective temperature of Eq. (8) with $M = 30$ at the fixed $\gamma_0^I = -0.000\,075$. Set II denoted by the gREM^{II} was performed with the scaled $\gamma_0^{II} = -0.000\,075 \times (64/L)^2$ and $M = 50$. Since the backbending region in $T_S(E)$ becomes flat with increasing L [see Fig. 9(b)], γ_0^{II} in the gREM^{II} is systematically lowered by the scaling factor $(64/L)^2$, producing more delocalized GPDFs and enhancing $p_{acc}(\alpha)$ for the transition region. Since the simulation with $L = 128$ in the gREM^I did not show statistically meaningful transitions, it was excluded in the scaling analysis.

The comparison of τ_E in Table III reveals that the speedup in N_E with increasing L is even more remarkable in both gREM^I and gREM^{II}. The ratio $R_\tau = \tau_E^{WL} / \tau_E^{gREM}$ increases from about 10^2 order at $L = 32$ to 10^4 order at $L = 128$. An apparent linear behavior in the log-log plot of L and τ_E is seen in the gREM^I of Fig. 9(a). The scaling behavior follows $\tau_E^I \simeq 0.047 \times L^{2d+0.5}$, implying that the acceleration of N_E in the gREM^I is about 10^2 order up to $L = 100$. When more crossing points are created in the phase transition region with $M = 50$, the growth of τ_E as a function of L is weaker, with a lower slope in the log-log plot in the gREM^{II}, yielding $\tau_E^{II} \simeq 0.156 \times L^{2d+0.0477}$. The scaling behavior of the gREM approaches that of a random walk in energy as more replicas are built up in the phase transition region.[57]

The profiles of $T_S(E)$ represented by the most probable energy set $[E_\alpha^*, T_\alpha^*]$ show a clear backbending for $L = 16$ and 32 in Fig. 9(b), but the extent of the backbending gradually declines with increasing L and becomes almost flat at $L = 128$. In contrast to the backbending in the microcanonical caloric curve, $T_S(E)$, the inverse of the internal energy, $T = U^{-1}(E)$, which corresponds to a caloric curve in the canonical ensemble, monotonically increases across the phase transition region, implying that statistical ensembles are not equivalent in finite size systems.[29,30]

TABLE III. Simulation parameters and mean tunneling times τ_E for the gREM^I and gREM^{II} simulations with varying L. The gREM^I simulations are associated with $\gamma_0^I = -0.000\,075$ and $M = 30$. The gREM$_7^*$ was performed with Eq. (13) based on $[E_\alpha^*, T_\alpha^*]$ of the gREM$_7$. τ_E^I and τ_E^{II} correspond to the gREM^I and gREM^{II}, respectively.

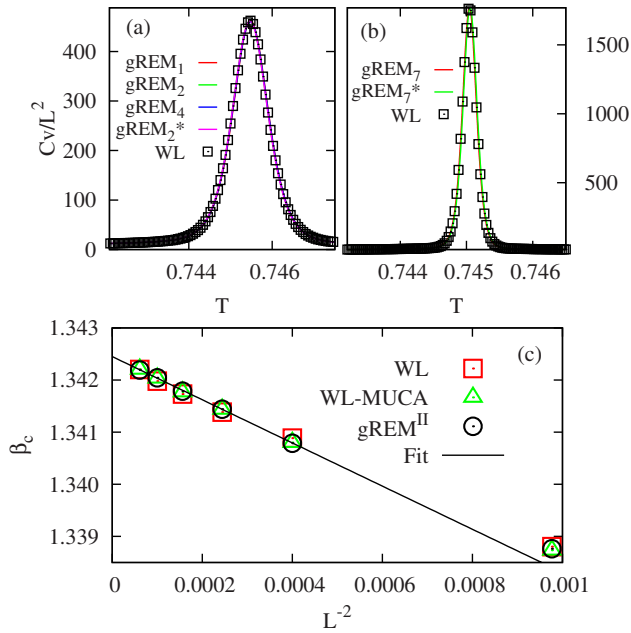| Methods	L	$\gamma_0^{II}(M=50)$	τ_E^I (MCS)	τ_E^{II} (MCS)	t_S (MCS)
gREM$_1$	16	−0.0012	48.1	43.7	1.0×10^7
gREM$_2$	32	−0.0003	274.7	224.2	7.0×10^7
gREM$_3$	50	−0.00012	851.0	487.1	1.5×10^8
gREM$_4$	64	−0.000075	1511.7	755.3	1.5×10^8
gREM$_5$	80	−0.000048	2710.2	1371.1	1.5×10^8
gREM$_6$	100	−0.000031	4739.1	1920.2	1.5×10^8
gREM$_7$	128	−0.0000187		2998.3	1.5×10^8
gREM$_7^*$	128	−0.0000038		139.5	1.5×10^8

FIG. 10. Heat capacities $C_v(T)$ around T_c of the WL-MUCA and various gREM simulations for Potts spins at (a) $L=64$ and (b) $L=128$, and plots of $\beta_c(L)$ with L^{-2} for the gREM^{II} in Table III, the WL, and the WL-MUCA simulations. In (b), the line is a linear fit to the data of the gREM^{II}.

E. Thermodynamics

After a sufficient long production run the gREM determines the entropy estimate, $\widetilde{S}(E)$, by joining multiple replica simulations via the WHAM.[55] Once $\widetilde{S}(E)$ is determined, all canonical thermodynamic properties, such as the internal energy, $U(T)$, and the heat capacity, $C_v(T)$, are completely determined. As demonstrated in Fig. 10(a), heat capacities (lines) determined by various gREM simulations in Table I for $L=64$ are collapsed into a single curve with good agreement with the WL-MUCA simulation (squares), irrespective of simulation conditions. Also, heat capacities at $L=128$ in Fig. 10(b) determined by both gREM$_7$ and gREM$_7^*$ in Table II are almost indistinguishable from that of the WL-MUCA even with a significantly shorter simulation time.

Here WL-MUCA denotes the MUCA sampling with the frozen $\widetilde{S}(E)$ refined by the WL up to $f_d=10^{-9}$. We found that thermodynamic properties determined by a bare $\widetilde{S}(E)$ gives a systematic discrepancy from those of the gREM simulations, as demonstrated in the plot of β_c with L^{-2} in Fig. 10(b). Indeed, it is found that energy distributions $P_{MU}(E)$ obtained by the MUCA sampling with the frozen $\widetilde{S}(E)$ for 10^8 MCS show a considerable deviation from a uniform sampling, implying that the WL $\widetilde{S}(E)$ still contains an error stemming from the refinement process.[59] We correct this error by applying the reweighting process for the entropy estimate as $\widetilde{S}_{MU}(E)=\widetilde{S}(E)+\ln P_{MU}(E)$. As shown in Figs. 10(a) and 10(b) the reweighted $\widetilde{S}_{MU}(E)$ produce thermodynamics consistent with that of the gREM.

At finite L the singularities and discontinuities in first-order phase transitions of infinite systems are smeared out,[60] and backbending emerges in $T_S(E)$. With increasing L, $T_S(E)$ becomes flat, rounded transitions transform into sharp ones,

and the size dependent critical temperature, $\beta_c(L)=1/T_c(L)$, approaches the thermodynamic transition temperature, $\beta_c^\infty =1/T_c^\infty$. This asymptotic behavior can be predicted by finite size scaling analysis[61] as

$$\beta_c(L) = \beta_c^\infty + 1/L^d, \qquad (14)$$

in which the critical temperature, $\beta_c(L)$, was determined as the temperature at the peak in $C_v(T)$.

As seen in Fig. 10(b), the critical temperatures determined by the gREM^{II} and the WL-MUCA are in quantitative agreement. Furthermore, plotting $\beta_c(L)$ versus L^{-2} yields a good straight line, extrapolating to $\beta_c^\infty =1.332\,447$, close to the exact $\ln(1+\sqrt{Q=8})=1.342\,454$.[56] On the other hand, a noticeable deviation from a linear fit shows up in the scaling behavior of $\beta_c(L)$ in the original WL. To eliminate finite size effects at a smaller L, we used the data set between $L=50$ and $L=120$ for a linear fit.

IV. CONCLUSIONS

The generalized Replica Exchange Method (gREM) has been developed to facilitate effective configurational sampling in systems exhibiting backbending, or an S-loop, in the statistical temperature, $T_S(E)$, characteristic of first-order phase transitions in finite systems. By combining optimally parametrized, generalized ensemble samplings with replica exchanges, our method enables a comprehensive sampling for phase transition regions with successive unimodal energy distributions, by transforming metastable or unstable energy states of canonical ensembles into stable ones. Exploiting the one-to-one correspondence between the sampling weight and the effective temperature, we also present an inverse mapping strategy, which determines optimal sampling weights from tailored effective temperatures, avoiding an intrinsic instability of the canonical ensemble to the negative slope region of $T_S(E)$.

The effectiveness of our method has been explicitly demonstrated for Potts spin systems, for various simulations conditions, as a function of the system size, L. The quantitative comparison between the gREM and WL sampling reveals that the gREM provides an order of magnitude acceleration of tunneling transitions over the WL, while maintaining a faithful sampling for the phase transition region as in flat histogram methods. The underlying mechanism for accelerated tunneling transitions is the capacity of the gREM to preserve mixed-phase configurations in intermediate replicas located at the transition region. Finite size scaling analysis shows that in the optimum case of the gREM, the scaling of the mean tunneling time, τ_E, approaches $\propto L^{2d}$, corresponding to the ideal limit of flat histogram methods. It is also shown that the gREM provides a correct canonical thermodynamics via the reweighting with a much smaller simulation time.

Finally, we would like to emphasize that the inverse mapping strategy is a general framework that can be applied to the combination of any generalized ensemble sampling and the replica exchange method. We anticipate that a hybrid extension augmented by the inverse mapping, applying the gREM to selective transition regions while retaining the

*t*REM for other energy regions, will allow the widespread use of our method to various systems with first-order transitions.

ACKNOWLEDGMENTS

[1] R. H. Swendsen and J. S. Wang, Phys. Rev. Lett. **57**, 2607 (1986).
[2] C. J. Geyer and A. Thompson, J. Am. Stat. Assoc. **90**, 909 (1995).
[3] K. Hukushima and K. Nemoto, J. Phys. Soc. Jpn. **65**, 1604 (1996).
[4] U. H. E. Hansmann, Chem. Phys. Lett. **281**, 140 (1997).
[5] Y. Sugita and Y. Okamoto, Chem. Phys. Lett. **314**, 141 (1999).
[6] R. Zhou and B. J. Berne, Proc. Natl. Acad. Sci. U.S.A. **99**, 12777 (2002); A. E. Garcia and J. N. Onuchic, *ibid.* **100**, 13898 (2003).
[7] R. Yamamoto and W. Kob, Phys. Rev. E **61**, 5473 (2000).
[8] P. A. Frantsuzov and V. A. Mandelshtam, Phys. Rev. E **72**, 037102 (2005).
[9] M. E. J. Newman and G. T. Barkema, *Monte Carlo Methods in Statistical Physics* (Clarendon, Oxford, 1999).
[10] Y. Sugita and Y. Okamoto, Chem. Phys. Lett. **329**, 261 (2000); A. Mitsutake, Y. Sugita, and Y. Okamoto, J. Chem. Phys. **118**, 6664 (2003); **118**, 6676 (2003).
[11] F. Calvo and J. P. K. Doye, Phys. Rev. E **63**, 010902 (2000).
[12] R. Faller, Q. Yan, and J. J. de Pablo, J. Chem. Phys. **116**, 5419 (2002).
[13] H. Fukunishi, O. Watanabe, and S. Takada, J. Chem. Phys. **116**, 9058 (2002).
[14] T. W. Whitfield, L. Bu, and J. E. Straub, Physica A **305**, 157 (2002).
[15] S. Jang, S. Shin, and Y. Park, Phys. Rev. Lett. **91**, 058305 (2003).
[16] P. Liu, B. Kim, R. A. Friesner, and B. J. Berne, Proc. Natl. Acad. Sci. U.S.A. **102**, 13749 (2005); P. Liu, X. Huang, R. Zhou, and B. J. Berne, J. Phys. Chem. B **110**, 19018 (2006).
[17] X. Cheng, G. Cui, V. Hornak, and C. Simmering, J. Phys. Chem. B **109**, 8220 (2005).
[18] E. Lyman, F. M. Ytreberg, and D. M. Zuckerman, Phys. Rev. Lett. **96**, 028105 (2006).
[19] F. Calvo, J. Chem. Phys. **123**, 124106 (2005).
[20] S. W. Rick, J. Chem. Phys. **126**, 054102 (2007).
[21] P. Liu and G. A. Voth, J. Chem. Phys. **126**, 045106 (2007).
[22] H. Kamberaj and A. van der Vaart, J. Chem. Phys. **127**, 234102 (2007).
[23] P. Brenner, C. R. Sweet, D. VonHandorf, and J. A. Izaguirre, J. Chem. Phys. **126**, 074103 (2007).
[24] C. Zhang and J. Ma, Phys. Rev. E **76**, 036708 (2007).
[25] S. Trebst, M. Troyer, and U. H. E. Hansmann, J. Chem. Phys. **124**, 174903 (2006).
[26] A. J. Ballard and C. Jarzynski, Proc. Natl. Acad. Sci. U.S.A. **106**, 12224 (2009).
[27] P. Kar, W. Nadler, and U. H. E. Hansmann, Phys. Rev. E **80**, 056703 (2009).
[28] D. J. Earl and M. W. Deem, Phys. Chem. Chem. Phys. **7**, 3910 (2005).
[29] H. Behringer and M. Pleimling, Phys. Rev. E **74**, 011108 (2006).
[30] D. H. E. Gross, Rep. Prog. Phys. **53**, 605 (1990).
[31] O. Lopez, D. Lacroix, and E. Vient, Phys. Rev. Lett. **95**, 242701 (2005).
[32] C. Junghans, M. Bachmann, and W. Janke, Phys. Rev. Lett. **97**, 218103 (2006).
[33] H. Hernández-Rojas and J. M. Gomez Llorente, Phys. Rev. Lett. **100**, 258104 (2008).
[34] J. Kim, T. Keyes, and J. E. Straub, Phys. Rev. E **79**, 030902(R) (2009).
[35] P. Labastie and R. L. Whetten, Phys. Rev. Lett. **65**, 1567 (1990).
[36] D. J. Wales and R. S. Berry, Phys. Rev. Lett. **73**, 2875 (1994).
[37] M. D'Agostino, F. Gulminelli, Ph. Chomaz, M. Bruno, F. Cannata, R. Bougault, F. Gramegna, I. Iori, N. Le Neindre, G. V. Margagliotti, A. Moroni, and G. Vannini, Phys. Lett. B **473**, 219 (2000).
[38] M. Schmidt, R. Kusche, T. Hippler, J. Donges, W. Kronmüller, B. von Issendorff, and H. Haberland, Phys. Rev. Lett. **86**, 1191 (2001).
[39] K. Huang, *Statistical Mechanics* (Wiley, New York, 1972).
[40] M. S. S. Challa and J. H. Hetherington, Phys. Rev. Lett. **60**, 77 (1988).
[41] T. Neuhaus, M. P. Magiera, and U. H. E. Hansmann, Phys. Rev. E **76**, 045701(R) (2007).
[42] J. Kim, Y. Fukunishi, and H. Nakamura, Phys. Rev. E **67**, 011105 (2003).
[43] J. Kim, Y. Fukunishi, A. Kidera, and H. Nakamura, Phys. Rev. E **68**, 021115 (2003).
[44] E. Heinsalu, R. Tammelo, and T. Örd, Phys. Rev. E **69**, 021111 (2004).
[45] J. Kim, Y. Fukunishi, and H. Nakamura, J. Chem. Phys. **121**, 1626 (2004).
[46] J. Kim, Y. Fukunishi, A. Kidera, and H. Nakamura, J. Chem. Phys. **121**, 5590 (2004).
[47] B. A. Berg and T. Celik, Phys. Rev. Lett. **69**, 2292 (1992); Phys. Lett. B **267**, 249 (1991).
[48] F. Wang and D. P. Landau, Phys. Rev. Lett. **86**, 2050 (2001); Phys. Rev. E **64**, 056101 (2001).
[49] J. Kim, J. E. Straub, and T. Keyes, Phys. Rev. Lett. **97**, 050601 (2006); J. Chem. Phys. **126**, 135101 (2007); Phys. Rev. E **76**, 011913 (2007).
[50] C. Tsallis, J. Stat. Phys. **52**, 479 (1988).
[51] I. Andricioaei and J. E. Straub, Phys. Rev. E **53**, R3055 (1996).
[52] I. Andricioaei and J. E. Straub, J. Chem. Phys. **107**, 9117 (1997).
[53] J. Kim and J. E. Straub, J. Chem. Phys. **130**, 144114 (2009).
[54] U. H. E. Hansmann and Y. Okamoto, Phys. Rev. E **56**, 2228 (1997).
[55] A. M. Ferrenberg and R. H. Swendsen, Phys. Rev. Lett. **63**, 1195 (1989).
[56] F. Y. Wu, Rev. Mod. Phys. **54**, 235 (1982); **55**, 315(E) (1983).
[57] P. Dayal, S. Trebst, S. Wessel, D. Wurtz, M. Troyer, S. Sabhapandit, and S. N. Coppersmith, Phys. Rev. Lett. **92**, 097201 (2004).
[58] J. Kim, T. Keyes, and J. E. Straub, J. Chem. Phys. **130**, 124112 (2009).
[59] C. Zhou and J. Su, Phys. Rev. E **78**, 046705 (2008).
[60] K. Binder and D. P. Landau, Phys. Rev. B **30**, 1477 (1984).
[61] A. Bazavov, B. A. Berg, and S. Dubey, Nucl. Phys. B **802**, 421 (2008).